

Recurrence in the high-order nonlinear Schrödinger equation: a low dimensional analysis

Andrea Armaroli,^{1,*} Maura Brunetti,¹ and Jérôme Kasparian¹

¹*GAP, Université de Genève, Chemin de Pinchat 22, 1227 Carouge, Switzerland*

(Dated: December 3, 2024)

We study a three-wave truncation of the high-order nonlinear Schrödinger equation for deep-water waves (HONLS, also named Dysthe equation). We validate our approach by comparing it to numerical simulation, distinguish the impact of the different fourth-order terms and classify the solutions according to their topology. This allows us to properly define the temporary spectral *upshift* occurring in the nonlinear stage of Benjamin-Feir instability and provides a tool for studying further generalizations of this model.

I. INTRODUCTION

Nonlinear Schrödinger equation (NLS) is a universal model which applies to deep-water waves, nonlinear optics, plasma physics and Bose-Einstein condensates among others[1, 2]. It is an integrable partial differential equation which gives us access to a set of powerful mathematical techniques[3, 4]. Nevertheless, it is based on a narrow-band approximation (i.e. derived by means of the slowly-varying envelope approximation or the method of multiple scales); many extensions were proposed to describe different situations and phenomena. Particularly, in hydrodynamics, where the wave steepness of the carrier plays the role of perturbation parameter, nearly 40 years ago a fourth-order generalization of the NLS was proposed in [5]. We denote this model high-order NLS (HONLS). The main drive to develop such a model was to better explain the properties of the ubiquitous Benjamin-Feir instability (BFI) [6, 7], i.e. the well-known growth of oscillations on top of a uniform Stokes wave. The spectral downshift observed in BFI [8] can be often explained in the HONLS framework. However, in the last decades much effort has been devoted to characterize the properties of this model and to include other effects, such as viscosity or wind [9–18].

As far as the mathematical properties of the HONLS are concerned, we recall that the conventional reference frame change, which allows one to write a time-like HONLS (where the evolution variable is space), leads to two different forms: the equation describing the evolution of the envelope of the surface elevation (thereafter denoted HONLS_e) and the one pertaining to the envelope of the velocity potential (HONLS_p). The former possesses less conservation laws than the latter: this is a consequence of the choice of canonical variables [19–22]. Nevertheless those variables can be less accessible from an experimental point of view.

No matter which form we consider, the HONLS exhibits nearly perfect recurrence of the initial state (a hint of an underlying integrable evolution); the conventional

wisdom is that during this cyclic behavior the spectral peak is downshifted while the spectral mean is upshifted [8, 23, 24].

In this work we will study the behavior of recurrence in the two forms of HONLS and characterize the origin of the temporary peak downshift. After having recalled in section II the main properties of the model, we present (section III) a three-wave truncation [25, 26, p. 527], by means of which we find a closed form for the equations which rule the nonlinear behavior of BFI, obtain an approximate one-degree-of-freedom phase space, where the evolution of experimental quantities can be mapped onto, and clarify what a sound definition of spectral shift should be.

This approach proved effective in other nearly-integrable systems [27], where exact solutions cannot be constructed. This is the case of HONLS: the Akhmediev breather [28, 29], the Peregrine soliton [30, 31], conventionally regarded as prototypes of rogue waves [32, 33], only represent approximate solutions [34]. The non-integrability appears nevertheless to be an important ingredient for the appearance of extreme events (e.g. in optical fibers [35, 36]).

II. HIGH-ORDER NONLINEAR SCHRÖDINGER EQUATIONS

A. Model equations

Let us start from the normalized time-like HONLS[5]

$$\frac{\partial a}{\partial \xi} + i \frac{1}{2} \frac{\partial^2 a}{\partial \tau^2} + i |a|^2 a = \epsilon \{ f[a] + \beta g[a] + h[a] \}, \quad (1)$$

where the adimensional quantities are obtained from dimensional ones as $a = A/A_0$, $\tau = t/T_0$, $\xi = x/L_0$. A is the complex envelope of surface elevation, t and x are time and propagation distance in a frame moving at the group velocity of the carrier wave. The normalization constant A_0 is chosen by setting a value of the steepness $\epsilon = A_0 k_0 / \sqrt{2}$, k_0 being the carrier wave-number. Finally $T_0 = 1/(\omega_0 \epsilon)$, $L_0 = 1/(2\epsilon^2 k_0)$ with $\omega_0 = \sqrt{g k_0}$ the angular frequency of the wave in the

* andrea.armaroli@unige.ch

limit of infinitely deep water. Thanks to those definitions, $a = \mathcal{O}(1)$ and ϵ controls the relative importance of higher-order corrections. We define $f[a] \equiv 8|a|^2 \frac{\partial a}{\partial \tau}$, $g[a] \equiv 2a^2 \frac{\partial a^*}{\partial \tau}$ and $h[a] \equiv 2ia\mathcal{H}\left[\frac{\partial |a|^2}{\partial \tau}\right]$ ($\mathcal{H}[\cdot]$ denotes the Hilbert transform). β is used to distinguish the HONLSe ($\beta = 1$) from the HONLSp ($\beta = 0$) [23]. This latter conserves not only the norm $N \equiv \int_{-\infty}^{\infty} |a|^2 d\tau$ (the only conserved quantity of HONLSe), but also the momentum $P \equiv \frac{i}{2} \int_{-\infty}^{\infty} (a_{\tau}^* a - a_{\tau} a^*) d\tau$ and the Hamiltonian $E \equiv E_0 - \epsilon E_1$, with $E_0 = \frac{1}{2} \int_{-\infty}^{\infty} (|a_{\tau}|^2 - |a|^4) d\tau$ and $E_1 = i \int_{-\infty}^{\infty} |a|^2 [2(a_{\tau}^* a - a_{\tau} a^*) - \mathcal{H}[|a|^2]_{\tau}] d\tau$.

B. Numerical analysis

We find it useful to briefly recall the properties of the full nonlinear evolution of BFI after the initial exponential growth phase. Since the excitation of a harmonically perturbed Stokes wave represents a good approximation of the Akhmediev breather, we solve the HONLSe with initial condition $a(0, \tau) = (1 - \sqrt{\eta}) + \sqrt{2\eta} \cos(\Omega\tau + \tilde{\phi})$, with $\tilde{\eta} = 1 \times 10^{-2}$, $\tilde{\phi} = \pi/4$ and $\Omega = \Omega_M = \sqrt{2}(1 - \frac{3}{2}\epsilon)$, i.e. the frequency of maximum instability growth, which depends only on the $h[a]$ contribution [5] (see also the derivation below). We use $\epsilon = \sqrt{2}/20$ as initial steepness. We numerically solve Eq. (1) by means of the 3rd-order Runge-Kutta (RK) scheme embedding the conventional 4th-order RK applied in the interaction picture formulation of the HONLSe [37]. In Fig. 1(a) we show the evolution of the Stokes wave and its lateral sidebands of first (the unstable modes, at $\pm\Omega$) and second order ($\pm 2\Omega$ generated by the four-wave mixing process $\omega_0 \pm \Omega + \omega_0 \pm \Omega + \omega_0 \rightarrow \omega_0 \pm 2\Omega$). The recurrence is almost perfect and can be separated in three phases: (i) the unstable modes grow with a predominant upshift, see the dash-dotted lines in panel (a) and also the blue line in Fig. 1(b), which corresponds to the sideband unbalance $\Pi \equiv \Omega(|\hat{a}(\Omega)|^2 - |\hat{a}(-\Omega)|^2)$ (\hat{a} is the Fourier-transform of a); (ii) the second order sidebands start growing due to four-wave mixing; this effect is unbalanced towards 2Ω (so that the spectral mean grows) and contributes to the opposite-side unstable mode ($-\Omega$) via four-wave mixing, thus we observe a peak downshift as soon as the Stokes wave is overcome by the unstable modes; (iii) at maximum conversion the process reverses to the initial perturbed plane wave.

In Fig. 1(b) we also plot the ratio of momentum and norm P/N . We can derive an integral expression for the evolution of this quantity as:

$$\frac{d}{d\xi} \frac{P}{N} = -2\beta\epsilon \frac{R}{N} \quad (2)$$

with $R \equiv \frac{i}{2} \int_{-\infty}^{\infty} |a|^2 (a_{\tau\tau}^* a - a_{\tau\tau} a^*) d\tau$.

If Π changes sign and unstable sidebands dominate over the Stokes wave, we can state that the spectral peak has shifted, so this variable describes what is the experimental peak frequency. Instead P/N is, by definition, an

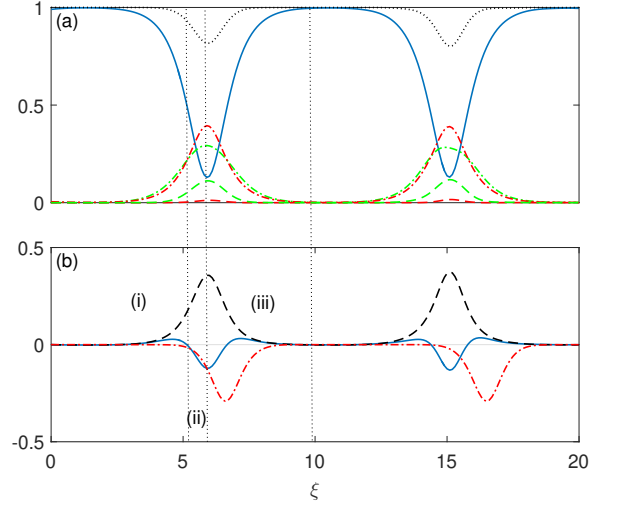


FIG. 1. (a) Numerical results of HONLSe simulations. Evolution of the squared amplitude of the Stokes wave (blue solid line), its unstable sideband pair ($\pm\Omega$, dash-dotted lines) and second order sidebands ($\pm 2\Omega$, dashed lines). Red (green) lines represent the low (high) frequency sideband. The black dotted line represent the sum of square amplitudes of Stokes wave and its unstable sidebands. (b) The corresponding relative unbalance of sideband amplitudes Π (solid blue for HONLSe, dash-dotted red in the HONLSp) and spectral shift P/N (dashed black, full HONLSe; not reported for HONLSp). The labels (i-iii) correspond to three stages of recurrence in HONLSe mentioned in the main text.

average over all stable and unstable modes and represents the spectral mean: in Fig. 1(b) we observe its temporary passage in the positive region for the HONLSe (black dashed line).

P is conserved for $\beta = 0$: it is thus apparent that $g[a]$ is associated to the temporary growth of P/N . The spectral peak downshift is instead observed in both models (compare blue solid and red dash-dotted lines in Fig. 1(b)), thus it can be associated to $f[a]$, which appears as an intensity-dependent increase of group velocity [23, 38]. As it was shown in [39, 40], this term induces an almost homogeneous drift in the recurrence. Given the dispersion relation, an increase in group velocity $C_g = g/(2\omega_0)$ is equivalent to a decrease in the instantaneous frequency. Beyond this qualitative explanation, a numerical analysis of the solutions of HONLSp allows us to fit, close to Ω_M , the maximum shift with $\Delta\Omega_{\max} = -3\epsilon(1 - 2(\Omega - \Omega_M))$: for a single unstable mode, less conversion to sidebands implies a smaller downshift. We will refer to the effect of $f[a]$ as kinematic.

Notice that the recurrence period exhibits (see Fig. 1(b)) a ($\simeq 10\%$) walk-off between HONLSe and HONLSp: here HONLSp lags behind HONLSe, but a different choice of the initial relative phase $\tilde{\phi}$ leads to either positive or negative differences. We also observe (Fig. 1(a)) that only a moderate proportion of the energy

is converted to higher-order sidebands (about 20%).

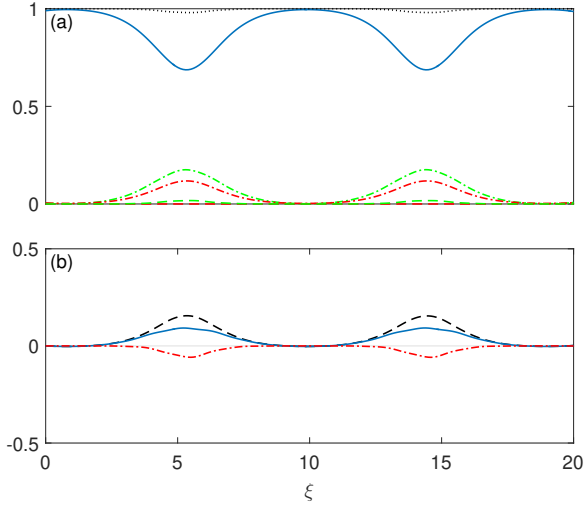


FIG. 2. Same as Fig. 1, but with $\Omega = 1.6$. Notice that the growth of unstable modes is much smaller and the kinematic peak downshift (still noticeable in HONLSe) cannot compensate the mean upshift in HONLSe.

Finally, we repeat the numerical experiment for a unstable frequency closer to the instability margin (see be-

low), i.e. $\Omega = 1.6$, where the BFI growth rate is smaller. The relative impact of unstable modes is reduced and the upshift for $\beta = 1$ dominates the always present kinematic downshift, see Fig. 2: notice that the blue line in panel (b) does not cross into negative values anymore.

III. THREE WAVE TRUNCATION

Given the limited conversion to higher-order sidebands, we conjecture that the dynamics of Eq. (1) can be captured by a dynamical system with a finite number of degrees of freedom. We assume a limited tank length or, equivalently, a careful temporal profile of the initial condition in order to prevent that the unavoidable mixing products (at $\pm n\Omega$, with integer n) generated during propagation fall inside the instability range. This single unstable mode regime corresponds to the following Ansatz

$$a(\xi, \tau) = A_0(\xi) + A_1(\xi)e^{-i\Omega\tau} + A_{-1}(\xi)e^{i\Omega\tau} \quad (3)$$

where A_0 thus describes the evolution of the Stokes wave complex amplitude, while $A_{\pm 1}$ are the amplitudes of the unstable sidebands.

By replacing the Ansatz of Eq. (3) inside Eq. (1) we obtain a system of three complex equations

$$\begin{aligned} \dot{A}_0 &= -i \left(|A_0|^2 + 2|A_1|^2 + 2|A_{-1}|^2 \right) A_0 - 2iA_0^*A_1A_{-1} \\ &\quad + i\epsilon\Omega \left\{ -8(|A_1|^2 - |A_{-1}|^2)A_0 + 4\beta(|A_1|^2 - |A_{-1}|^2)A_0 + 2s \left[(|A_{-1}|^2 + |A_1|^2)A_0 + 2A_0^*A_{-1}A_1 \right] \right\} \\ \dot{A}_1 &= i\frac{\Omega^2}{2}A_1 - i \left(|A_1|^2 + 2|A_0|^2 + 2|A_{-1}|^2 \right) A_1 - iA_0^2A_{-1}^* \\ &\quad + i\epsilon\Omega \left\{ -8(|A_0|^2 + |A_1|^2)A_1 + 2\beta(|A_1|^2 - 2|A_{-1}|^2)A_1 - 2\beta A_0^2A_{-1}^* + 2s \left[(|A_0|^2 + 2|A_{-1}|^2)A_1 + A_0^2A_{-1}^* \right] \right\} \\ \dot{A}_{-1} &= i\frac{\Omega^2}{2}A_{-1} - i \left(|A_{-1}|^2 + 2|A_0|^2 + 2|A_1|^2 \right) A_{-1} - iA_0^2A_1^* \\ &\quad + i\epsilon\Omega \left\{ 8(|A_0|^2 + |A_{-1}|^2)A_{-1} - 2\beta(|A_{-1}|^2 - 2|A_1|^2)A_{-1} + 2\beta A_0^2A_1^* + 2s \left[(|A_0|^2 + 2|A_1|^2)A_{-1} + A_0^2A_1^* \right] \right\} \end{aligned} \quad (4)$$

The dot denotes the derivative in ξ and, stemming from $h[a]$, $s = \text{sign } \Omega$. It is easy to verify that $U = |A_0|^2 + |A_1|^2 + |A_{-1}|^2$ is conserved ($\dot{U} = 0$).

A. BFI sidebands

In the limit $|A_{\pm 1}| \ll |A_0|$ and $A_0(\xi) = \sqrt{U_0} \exp(-iU_0\xi)$, posing $A_{\pm 1} = u_{\pm 1} \exp(-iU_0\xi)$, we obtain the linearized system for $\mathbf{u} = [u_1, u_{-1}^*]^T$, $\dot{\mathbf{u}} = i\Sigma\mathbf{u}$,

with

$$\Sigma \equiv \begin{bmatrix} \frac{\Omega^2}{2} - U_0 - (8 - 2s)\epsilon\Omega U_0 & -U_0(1 - 2(s - \beta)\epsilon\Omega) \\ U_0(1 - 2(s + \beta)\epsilon\Omega) & -\frac{\Omega^2}{2} + U_0 - (8 + 2s)\epsilon\Omega U_0 \end{bmatrix}, \quad (5)$$

which permits to recover the well-known dispersion relation ($\mathbf{u} \sim \exp(i\kappa\xi)$), at order ϵ

$$\kappa \approx -8\epsilon\Omega\eta_0 \pm \frac{1}{2}|\Omega| \left[(\Omega^2 - 4U_0(1 - 2s\epsilon\Omega)) \right]^{\frac{1}{2}}$$

Thus the peak linear gain $g_M = U_0(1 - 2\epsilon\sqrt{2U_0})$ occurs for $\Omega_M \approx \pm\sqrt{2U_0}(1 - \frac{3}{2}\sqrt{2U_0}\epsilon)$ (i.e. the value employed

in the above simulations, Fig. 1); we also recover that the instability bandwidth (where $\text{Im } \kappa \neq 0$) shrinks to $[0, 2\sqrt{U_0}(1 - 2\sqrt{U_0}\epsilon)]$ due to $h[a]$, as it is well-known since the original presentation of the Eq. (1) [5, 23].

An often disregarded aspect is the symmetry of sidebands. The eigenvector of the matrix Σ corresponding to the faster-growing mode (i.e. the eigenvector direction at Ω_M) is $|u_1/u_{-1}|_M \approx 1 + 2\beta\epsilon\sqrt{2U_0}$, so for $\beta = 0$ the growth of BFI is symmetric. We thus can assert that $g[a]$ is responsible for the asymmetry of the sideband growth, favoring the up-shifted mode. This is consistent with the nonconservation of P mentioned above.

B. Reduction to one degree of freedom

We study the nonlinear stage of BFI, assuming now $U_0 = 1$. From the analysis presented above, the one unstable mode regime corresponds to $\Omega \geq 1 - 2\epsilon$ (upper half of the instability bandwidth). By taking $A_m(\xi) = \sqrt{\eta_m(\xi)} \exp(i\phi_m(\xi))$ ($m = 0, \pm 1$), we can show that the system (4) can be reduced to three variables, namely the sideband amplitude $\eta = \eta_1 + \eta_{-1} = 1 - \eta_0$, the relative phase $\psi = (\phi_1 + \phi_{-1} - 2\phi_0)/2$ and the sideband unbalance $\alpha = \eta_1 - \eta_{-1}$. If $\beta = 0$, $\dot{\alpha} = 0$ and Eq. (4) can be reduced to an integrable one-degree-of-freedom system in the canonical variables (η, ψ) ($\dot{\eta} = \frac{\partial H}{\partial \psi}$, $\dot{\psi} = -\frac{\partial H}{\partial \eta}$), with Hamiltonian

$$H(\psi, \eta) = -\left(\frac{\Omega^2}{2} - \sigma + \epsilon 4\Omega\alpha\right)\eta - \frac{3}{4}\eta^2 + \epsilon s\Omega\eta^2 + \sigma(1 - \eta)[\eta^2 - \alpha^2]^{\frac{1}{2}} \cos 2\psi \quad (6)$$

with $\sigma = (1 - 2s\epsilon\Omega)$. This integrable one degree-of-freedom reduction represents only a minor correction to the conventional NLS truncation [26], where $\sigma = 1$. Thus the phase space possesses a separatrix which distinguishes between two regimes: closed orbits inside the separatrix, which correspond to period-one recurrence, and open orbits which correspond to period-two (or phase-shifted) recurrence [28, 41, 42], see also the insets in Fig. 4 below.

The $\beta \neq 0$ case is ruled by

$$\begin{aligned} \dot{\eta} &= -2\sigma(1 - \eta)[\eta^2 - \alpha^2]^{\frac{1}{2}} \sin 2\psi \\ \dot{\psi} &= \frac{\Omega^2}{2} - 1 + \frac{3}{2}\eta + 2\epsilon\Omega\left(s(1 - \eta) + \frac{4 - \beta}{2}\alpha\right) \\ &\quad + \sigma[\eta^2 - \alpha^2]^{\frac{1}{2}} \cos 2\psi \\ &\quad - \sigma\eta(1 - \eta)[\eta^2 - \alpha^2]^{-\frac{1}{2}} \cos 2\psi + \\ &\quad + 2\beta\epsilon\Omega(1 - \eta)\alpha[\eta^2 - \alpha^2]^{-\frac{1}{2}} \cos 2\psi \\ \dot{\alpha} &= -4\beta\epsilon\Omega(1 - \eta)[\eta^2 - \alpha^2]^{\frac{1}{2}} \sin 2\psi \end{aligned} \quad (7)$$

The non-conservation of momentum in Eq. (1), see Eq. (2), is reflected to a non-conserved unbalance of the sidebands and a modification of the phase dynamics. Both

effects are perturbative, $\mathcal{O}(\epsilon)$, but have a measurable impact on the system evolution. Importantly we obtain a closed form for $\dot{\alpha}$, thus simplifying the qualitative and quantitative understanding of the evolution of HONLS and its further extensions.

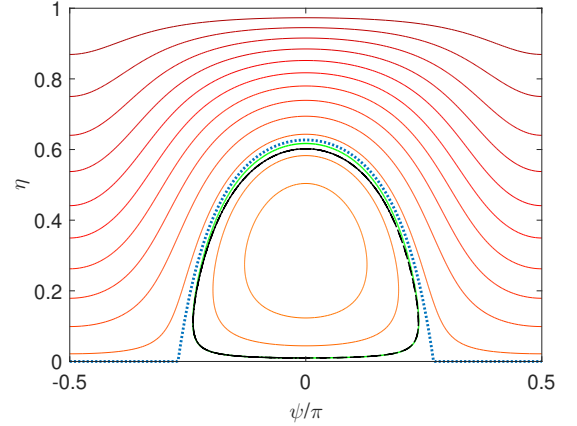


FIG. 3. Representation of the curves of constant H (level sets, Eq. (6)) in phase plane (ψ, η) . The dotted blue line represents the separatrix ($H = 0$); the level set corresponding to $\eta(0) = 0.01$, $\psi(0) = 0$, $\epsilon = \sqrt{2}/20$ is shown in green, while the dashed black line represents the actual solution of Eq. (7). Notice that the superposition of the curves is almost perfect everywhere.

In order to assess the deviation from integrability, we take $\eta(0) = 0.01$, $\psi(0) = 0$, $\alpha(0) = 0$, $\beta = s = 1$, $\epsilon = \sqrt{2}/20$ and compare the solution of Eq. (7) with the level sets of H , Fig. 3: albeit the non-conservation of α represents a sideband unbalance, it does not change the topology of the phase space (it is non-resonant).

C. Comparison to simulations

The relevance of the truncated model is further validated by comparing its solutions to the evolution of the sidebands according to the HONLS and to the truncated model. We use the same parameters as above, apart from the phase, for which we show the two different families of solutions (period-one for $\psi(0) = 0$, period-two for $\psi(0) = \pi/2 \bmod \pi$). In Fig. 4 we plot the HONLS results in the three-wave phase-space. The degree of superposition between the level sets of H defined above and the HONLS solutions is quantitatively good only for conversion to higher-order sidebands smaller than 10%, but the topology is completely preserved. As soon as a significant amount of energy is transferred to modes at $\pm 2\Omega$, the discrepancy grows. We verified numerically that the period of recurrence is under- or over-estimated by less than 10% (around the maximum conversion frequency, not shown).

Larger values of steepness ($\epsilon > 0.2$, not shown) severely break the conservation of P/N and, after 3 or more recur-

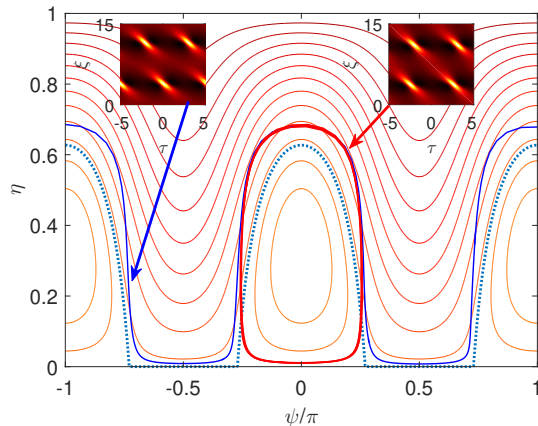


FIG. 4. Representation of solutions of HONLSe on the phase plane of the one degree-of-freedom model of Fig. 3. The red line correspond to the inside of the separatrix ($\psi(0) = 0$, *period-one*), the blue line to the outside ($\psi(0) = \pi/2$, *period-two*). In spite of a deviation from three-wave truncation, the topology is conserved. The two insets represent $|a|^2$ in the (τ, ξ) plane. As indicated by arrows, the “phase-shifted” solution (top-left) corresponds to the blue curve on the phase space; the top-right to the red curve, i.e. non-phase shifted solution.

rence cycles, can sporadically break the regularity of the evolution and lead to the crossing of the separatrix. For those values, anyway, the steep pulses attained during the breathing cycle ($|a| \approx 3$) greatly enhance the probability of wave-breaking, so that the physics is beyond the validity range of Eq. (1).

Then it is important to investigate the predictability of the spectral shift. In Fig. 5 we show the spectral mean

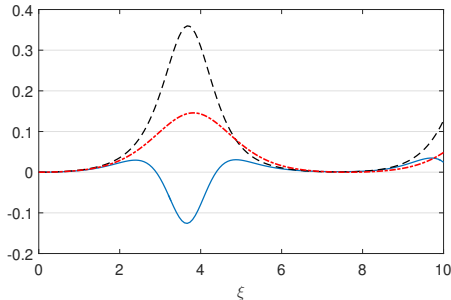


FIG. 5. Comparison of the peak spectral shifts Π and Π_3 obtained, respectively, from the full HONLS simulation (blue solid line) and the truncated three-wave model (red dash-dotted line). The spectral mean P/N is also shown (black dashed line). $\psi(0) = 0$ while all other parameters are as above.

$\Pi_3 \equiv \Omega\alpha$ for the truncated model along with its value P/N and the peak shift Π extracted from simulations. As we showed in Fig. 1, the spectral peak exhibits a upshift/downshift transition. This is ascribed to the $f[a]$ contribution, which in turn enters in Eq. (7) as a pure

phase shift, so it cannot provide a net effect on α . Despite Π_3 resembles Π in its definition, it describes instead the sideband unbalance caused by $g[a]$ in the three-mode truncation (the dash-dotted line approximates the dashed curve of P/N).

This consolidates the view that a definition of spectral shift cannot rely on the spectral peak position: this in turn depends on the definition of the reference frame (a correction of group velocity) rather than on dynamical effects (the privileged direction of four-wave mixing, which on average points towards higher frequencies).

The correct definition of (here temporary) up(down)-shift must thus rely on the P/N dynamics, which is notably appropriately described even by our low-dimensional approximation. The inclusion of more Fourier components (we verified it in the five-wave truncation) only slightly improves the approximation: the kinematic effect depends thus on a complex interplay of many (but not all) stable and unstable modes, while the spectral shift is a global average property. As shown above, by comparing Figs. 1 and 2, for a smaller BFI gain the conversion to higher-order modes is smaller and the upshift is dominant, consistently with our analysis.

IV. CONCLUSIONS

We analyzed a low-dimensional truncation of the so-called Dysthe equation in its two versions: the one which conserves only the norm (envelope HONLS) and the one which conserves also momentum and Hamiltonian (potential HONLS). This latter naturally reduces to a one degree-of-freedom integrable Hamiltonian system, while the former includes a closed-form non-resonant perturbation which breaks the integrability, but not the heteroclinic behavior. This low dimensional (albeit non-integrable) system of ODEs permits to model correctly the *spectral upshift* in the spectral-mean sense of the nonlinear stage of BFI and to distinguish it from other kinematic corrections, which manifest themselves as a frequency downshift.

While we could think to eliminate the term breaking the integrability of the system by means of a gauge transformation [22], this complicates however the analysis and the comparison to experimental results.

This approach is general and can be applied to other corrections of the NLS and HONLS, such as linear or nonlinear gain or dissipation, in order to ease the interpretation of the complex experimental data collected in the hundred meter long wave-tanks which are being currently developed.

ACKNOWLEDGMENTS

We acknowledge the financial support from the Swiss National Science Foundation (Project No. 200021-155970) We would like to thank Debbie Eeltink and John

-
- [1] A. R. Osborne, *Nonlinear ocean waves and the inverse scattering transform*, (Academic Press, 2009)
- [2] C. Sulem and P.-L. Sulem, *The Nonlinear Schrödinger Equation: Self-Focusing and Wave Collapse (Applied Mathematical Sciences)*, 1st ed. (Springer, 1999)
- [3] V. E. Zakharov and A. B. Shabat, “Exact Theory of Two-dimensional Self-focusing and One-dimensional Self-modulation of Wave in Nonlinear Media,” *Sov. Phys.—JETP* **34**, 62–69 (1972)
- [4] G. Biondini and D. Mantzavinos, “Universal Nature of the Nonlinear Stage of Modulational Instability,” *Phys. Rev. Lett.* **116**, 1–5 (2016)
- [5] K. B. Dysthe, “Note on a Modification to the Nonlinear Schrödinger Equation for Application to Deep Water Waves,” *Proc. R. Soc. A* **369**, 105–114 (1979)
- [6] T. B. Benjamin and J. E. Feir, “The disintegration of wave trains on deep water Part 1. Theory,” *J. Fluid Mech.* **27**, 417 (1967)
- [7] V. E. Zakharov and L. A. Ostrovsky, “Modulation instability: The beginning,” *Phys. D* **238**, 540–548 (2009)
- [8] B. M. Lake, H. C. Yuen, H. Rungaldier, and W. E. Ferguson, “Nonlinear deep-water waves: theory and experiment. Part 2. Evolution of a continuous wave train,” *J. Fluid Mech.* **83**, 49–74 (1977)
- [9] J. W. Miles, “On the generation of surface waves by shear flows,” *J. Fluid Mech.* **3**, 185 (1957)
- [10] F. Dias, A. I. Dyachenko, and V. E. Zakharov, “Theory of weakly damped free-surface flows: A new formulation based on potential flow solutions,” *Phys. Lett. A* **372**, 1297–1302 (2008)
- [11] J. Touboul and C. Kharif, “Nonlinear evolution of the modulational instability under weak forcing and damping,” *Nat. Hazards Earth Sys. Sci.* **10**, 2589–2597 (2010)
- [12] M. Onorato and D. Proment, “Approximate rogue wave solutions of the forced and damped nonlinear Schrödinger equation for water waves,” *Phys. Lett. A* **376**, 3057–3059 (2012)
- [13] M. Brunetti and J. Kasparian, “Modulational instability in wind-forced waves,” *Phys. Lett. A* **378**, 3626–3630 (2014)
- [14] M. Brunetti, N. Marchiando, N. Berti, and J. Kasparian, “Nonlinear fast growth of water waves under wind forcing,” *Physics Letters A* **378**, 1025–1030 (2014)
- [15] C. M. Schober and M. Strawn, “The effects of wind and nonlinear damping on rogue waves and permanent downshift,” *Physica D: Nonlinear Phenomena* **313**, 81–98 (2015)
- [16] J. D. Carter and A. Govan, “Frequency downshift in a viscous fluid,” *Eur. J. Mech. B* **59**, 177–185 (2016),
- [17] A. Toffoli, D. Proment, H. Salman, J. Monbaliu, F. Frascoli, M. Dafilis, E. Stramignoni, R. Forza, M. Manfrin, and Miguel Onorato, “Wind generated rogue waves in an annular wave flume,” (accepted by *Phys. Rev. Lett.* 2017),
- [18] D. Eeltink, A. Lemoine, H. Branger, O. Kimmoun, C. Kharif, J. D. Carter, A. Chabchoub, M. Brunetti, and J. Kasparian, “Spectral up- and downshifting of unstable Stokes waves under wind forcing,” submitted to *J. Fluid Mech.* (2017)
- [19] V. E. Zakharov, “Stability of periodic waves of finite amplitude on the surface of a deep fluid,” *J. Appl. Mech. Tech. Phys.* **9**, 190–194 (1968)
- [20] M. Stiassnie and L. Shemer, “On modification of the Zakharov equation for surface gravity waves,” *J. Fluid Mech.* **143**, 47–67 (1984)
- [21] O. Gramstad and K. Trulsen, “Hamiltonian form of the modified nonlinear Schrödinger equation for gravity waves on arbitrary depth,” *J. Fluid Mech.* **670**, 404–426 (2011)
- [22] F. Fedele and D. Dutykh, “Hamiltonian form and solitary waves of the spatial Dysthe equations,” *JETP Lett.* **94**, 840–844 (2012)
- [23] E. Lo and C. C. Mei, “A numerical study of water-wave modulation based on a higher-order nonlinear Schrödinger equation,” *J. Fluid Mech.* **150**, 395–416 (1985)
- [24] M. P. Tulin and T. Waseda, *J. Fluid Mech.*, Vol. 378 (1999) 197–232
- [25] G. B. Whitham, *Linear and Nonlinear Waves* (Wiley-Interscience, 1999)
- [26] S. Trillo and S. Wabnitz, “Dynamics of the nonlinear modulational instability in optical fibers,” *Opt. Lett.* **16**, 986–8 (1991)
- [27] M. Conforti, A. Mussot, A. Kudlinski, S. Rota Nodari, G. Dujardin, S. De Bièvre, A. Armaroli, and S. Trillo, “Heteroclinic Structure of Parametric Resonance in the Nonlinear Schrödinger Equation,” *Phys. Rev. Lett.* **117**, 013901 (2016)
- [28] N. N. Akhmediev, V. M. Eleonskii, and N. E. Kulagin, “Exact first-order solutions of the nonlinear Schrödinger equation,” *Theor. Mat. Phys.—JETP* **72**, 809–818 (1987)
- [29] A. Chabchoub, B. Kibler, J. M. Dudley, and N. N. Akhmediev, “Hydrodynamics of periodic breathers,” *Phil. Trans. R. Soc. A* **372**, (2014)
- [30] D. H. Peregrine, “Water waves, nonlinear Schrödinger equations and their solutions,” *J. Austral. Math. Soc. B* **25**, 16 (1983)
- [31] B. Kibler, J. Fatome, C. Finot, G. Millot, F. Dias, G. Genty, N. N. Akhmediev, and J. M. Dudley, “The Peregrine soliton in nonlinear fibre optics,” *Nat. Phys.* **6**, 790–795 (2010)
- [32] Nail N. Akhmediev, J. M. Soto-Crespo, and Adrian Ankiewicz, “Extreme waves that appear from nowhere: On the nature of rogue waves,” *Physics Letters A* **373**, 2137–2145 (2009)
- [33] John M. Dudley, Frédéric Dias, Miro Erkintalo, and Goëry Genty, “Instabilities, breathers and rogue waves in optics,” *Nature Photonics* **8**, 755–764 (2014)
- [34] V. E. Zakharov and A. I. Dyachenko, “About shape of giant breather,” *European Journal of Mechanics, B/Fluids* **29**, 127–131 (2010)
- [35] D. R. Solli, C. Ropers, P. Koonath, and B. Jalali, “Optical rogue waves,” *Nature* **450**, 1054–7 (2007)
- [36] A. Armaroli, C. Conti, and F. Biancalana, “Rogue solitons in optical fibers: a dynamical process in a complex energy landscape?” *Optica* **2**, 497 (2015)

- [37] S. Balac and Fabrice Mahé, “Embedded Runge-Kutta scheme for step-size control in the interaction picture method,” *Computer Phys. Comm.* **184**, 1211–1219 (2013)
- [38] A. Goullet and W. Choi, “A numerical and experimental study on the nonlinear evolution of long-crested irregular waves,” *Phys. Fluids* **23**, 1–15 (2011)
- [39] T. R. Akylas, “Higher-order modulation effects on solitary wave envelopes in deep water,” *J. Fluid Mech.* **198**, 387–397 (1989)
- [40] H. D. Zhang, C. Guedes Soares, and M. Onorato, “Modelling of the spatial evolution of extreme laboratory wave Heights with the nonlinear Schrödinger and Dysthe equations,” *Ocean Eng.* **89**, 1–9 (2014)
- [41] N. N. Akhmediev and V. I. Korneev, “Modulation instability and periodic solutions of the nonlinear Schrödinger equation,” *Theor. Math. Phys. –JETP* **69**, 1089–1093 (1986)
- [42] O. Kimmoun, H. C. Hsu, H. Branger, M. S. Li, Y. Y. Chen, C. Kharif, M. Onorato, E. J. R. Kelleher, B. Kibler, N. N. Akhmediev, and A. Chabchoub, “Modulation Instability and Phase-Shifted Fermi-Pasta-Ulam Recurrence,” *Sci. Rep.* **6**, 28516 (2016)

